Demonstration of nonperturbative and perturbative third-harmonic generation in MgO by altering the electronic structure

Mukhtar Hussain [1,*] Fernando Lima,[1] Willem Boutu [2] Hamed Merdji,[2] Marta Fajardo,[1] and Gareth O. Williams[1,†]

[1]*GoLP/Instituto de Plasmas e Fusão Nuclear-Laboratório Associado, Instituto Superior Técnico, Universidade de Lisboa, 1049-001 Lisboa, Portugal*

[2]*LIDYL, CEA, CNRS, Université Paris-Saclay, CEA Saclay, 91191 Gif-sur-Yvette, France*

The surge of interest in nonperturbative high-harmonic generation in solids has been driven by the appeal of compact solid-state extreme ultraviolet sources and the prospect of untangling the material properties through high-harmonic generation response to strong fields. The traditional assumption is that the brighter, lower-order harmonics are purely perturbative in nature. However, the border between the perturbative and nonperturbative regimes often remains unclear. Here, we show that third-harmonic generation (THG) using 800-nm, 40-fs pulses displays a nonperturbative response in a wide-band-gap insulator MgO. Furthermore, we show that with the introduction of dopants, the nonperturbative THG reverts to the perturbative behavior. We attribute this to the blocking of intraband oscillations and the increased linear absorption pathways introduced by the dopant energy levels.

I. INTRODUCTION

High-harmonic generation (HHG) is a robust method to up-convert near-infrared or visible light into extreme ultraviolet or even soft x rays in gases and solids [1,2]. In solids, the up-conversion of driving photon energies at moderate laser intensities due to the nonlinear polarizability of the medium is known as perturbative harmonic generation [3]. In this regime, the harmonic-generation efficiency falls off rapidly with increasing order [4]. More recently, HHG was realized in the strong-field regime, where electron tunneling, interband transitions, and intraband electron motion lead to nonperturbative harmonic generation [2,5–8]. These processes are typically associated with higher-order harmonics in the flat "plateau" region of the harmonic spectrum. Such harmonics have shown an intriguing dependence on the driving-field orientation [6,9,10], band structure [8], and intraband electron motion [6,8].

In nonperturbative high-harmonic generation (NP-HHG) studies, the lower-order harmonics are normally assumed to be perturbative and are largely ignored. The mechanism of NP-HHG for the low-order harmonics is generally due to intraband currents [11]. In the low-order harmonics, third-harmonic generation (THG) has been shown to display some characteristics of NP-HHG at high field strengths with 800-nm [12] and 1.3-μm [6] driving wavelengths. At longer driving wavelengths, the perturbative response persists at high field strengths [6], making the two regimes difficult to untangle through THG. The third harmonic (TH) is the brightest harmonic in centrosymmetric media that is still easy

to manipulate in air. Therefore, if NP-HHG can be clearly demonstrated in THG, it would be an attractive candidate for NP-HHG studies in solids.

If the origin of NP-HHG is well known, such as intraband motion in the conduction band, the harmonic emission can be traced to the shape of the band. Mapping the HHG emission as a function of crystal orientation and driving field can therefore yield information about the band shape and also map changes to that shape.

However, the role of the material properties in NP-HHG and its impact on the generation mechanism remain an open question. In particular, how the electronic structure influences the harmonic-generation mechanism is not yet fully understood. This understanding is crucial to know what information can be gleaned from solid-state harmonics in the perturbative regime. This was highlighted by a recent study of chromium-doped MgO, showing an increase in higher-order HHG emission [13] and lower-order harmonics [14] with altered electronic structures.

Here, we show that in a large-band-gap crystal, MgO, THG displays largely nonperturbative behavior. We identify the THG process by altering the electronic structure of MgO by doping it with chromium ions. We find that at the highest Cr concentration, the nonperturbative response reverts to the purely perturbative regime. We attribute this behavior to the changing electronic structure of the material with dopant concentration. This work shows that THG generation can carry all the hallmarks of a nonperturbative process that involves electron motion beyond the parent atom.

II. EXPERIMENTAL SETUP

Near-infrared (NIR) laser pulses at a wavelength of 800 nm and 40 fs in duration were focused on MgO crystals to generate the TH. An illustration of the experimental setup is

---

*Also at Department of Physics, University of Central Florida, Florida 32816, USA; mukhtar.hussain@ucf.edu
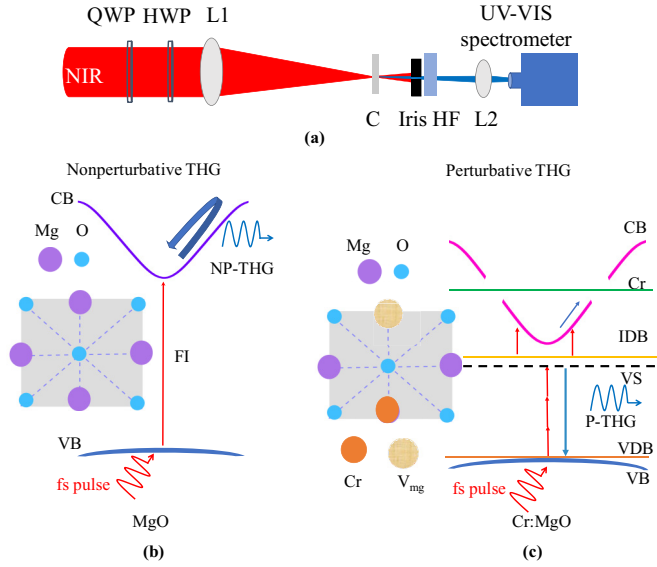
†gareth.williams@tecnico.ulisboa.pt

FIG. 1. (a) Schematic illustration of the experimental setup for THG in pure and CrMgO crystals showing the half-wave plate (HWP), quarter-wave plate (QWP), convex lenses (L1 and L2), crystals (C), and harmonic filter (HF); the iris is used to block the scattered NIR. (b) Band-diagram illustration of nonperturbative THG showing field ionization (FI) between the valence band (VB) and conduction band (CB); the intraband electron motion in the CB of pristine MgO results in the emission of TH signal. The inset shows the single unit cell of MgO. (c) Band-diagram illustration of perturbative THG in CrMgO, showing THG occurring either between the virtual state (VS) and the vacancy defect band (VDB) or VB. A single-photon linear absorption occurs between the IDB and the CB, and CB is split by higher Cr levels (Cr). The inset shows a single unit cell of CrMgO; V_{mg} represents the vacancy of Mg.
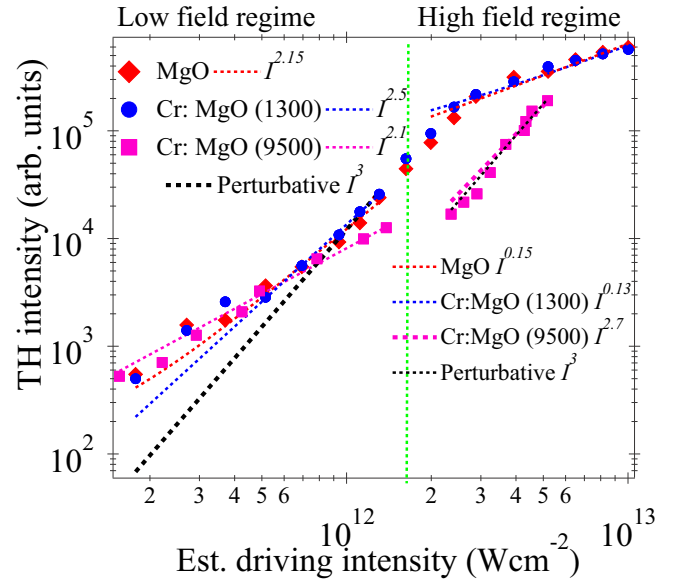

FIG. 2. The yield of TH in two regimes (low and high) in MgO (red diamonds), Cr:MgO (1300 ppm, blue dots), and Cr:MgO (9500 ppm, pink squares) versus the estimated driving intensity I. The power-law fitting in the low regime gives an exponent value of 2.15 (red dotted line) for MgO, 2.5 (blue dotted line) for Cr:MgO (1300 ppm), and 2.1 (pink dotted line) for Cr:MgO (9500 ppm), and for high regime it gives exponent values of 0.15, 0.13, and 2.7 for MgO, Cr:MgO (1300), and Cr:MgO (9500), respectively. We have controlled the intensity of the driving field by varying the diameter of an aperture which can induce an estimated error of ± 0.3 in the slope of harmonics.

shown in Fig. 1(a). Driving-field pulses of energy ≈ 20 μJ are focused to an ≈ 100-μm-diameter spot with a 75-cm lens onto 200-μm-thick pure MgO and Cr-doped MgO (Cr:MgO) crystals. The peak intensity is estimated to be $\approx 1.0 \times 10^{13}$ W cm^{-2}. The crystals are oriented along the (100) edge with a 001 cut. Tailored crystals (Cr:MgO) with different Cr doping concentrations (740, 1300, 5000, and 9500 ppm) were used. After the crystal, the THG pulses are filtered by a harmonic filter and focused by a convex lens (L2) with a 10-cm focal length onto a UV-VIS spectrometer [see Fig. 1(a)].

III. RESULTS AND DISCUSSION

A. Intensity dependence and doping impact on the yield of THG

The intensity variation of THG in pure MgO and Cr-doped MgO versus the estimated driving-field intensity is illustrated in Fig. 2 in the low- and high-field regimes. A perturbative TH process typically scales as I^3, where I is the driving intensity (shown by black dotted lines in Fig. 2). In the low-driving-intensity regime ($\leqslant 10^{12}$ W cm^{-2}), the responses of THG yield in MgO and Cr-doped MgO are quite similar ($I^{2.1}$ to $I^{2.5}$) and close to the expected I^3 dependence expected in perturbative THG. However, in the high-field regime where the intensity of the driving field is greater than 10^{12} W cm^{-2},

the dependence of THG intensity changes abruptly for the different crystals. The $I^{0.15}$ and $I^{0.13}$ dependences of MgO and Cr:MgO (1300 ppm) are shown in Fig. 2, which is more characteristic of a nonperturbative mechanism. This response indicates a nonperturbative scaling for MgO and low-doped MgO and a perturbative response in higher-doped MgO (9500 ppm; $I^{2.7 \pm 0.2}$) in the high-field regime.

The yield of the TH versus the concentration of Cr in MgO at $\approx 1.0 \times 10^{13}$ W cm^{-2} is shown in Fig. 3 (red diamonds). There is a sharp decrease (≈ 3.5 times) in the intensity of THG in Cr:MgO crystals for 740 ppm and a further reduction (≈ 5.5 times) for 1300 ppm. The efficiency decreases even more for higher dopant concentrations. To untangle the contributions of linear and nonlinear optical properties to the decrease in TH intensity as dopants are introduced, we have measured the linear optical properties at the TH wavelength through the pure and Cr-doped crystals. The linear transmission of the NIR transmission (black squares) and transmission of TH (blue dots) in MgO and Cr:MgO crystals are shown in Fig. 3 and follow closely the TH intensity (red diamonds). The decrease in the intensity of THG in Cr:MgO with the doping concentration is attributed to the increased absorption of the TH photons generated in the bulk of the doped crystals. This increased absorption is rooted in the altered electronic structure of the Cr:MgO crystals, which allows photon absorption between the virtual state (VS) and the conduction band (CB) transition [see Fig. 1(c)]. Additional electronic states such as the impurity defect band (IDB) and vacancy defect band
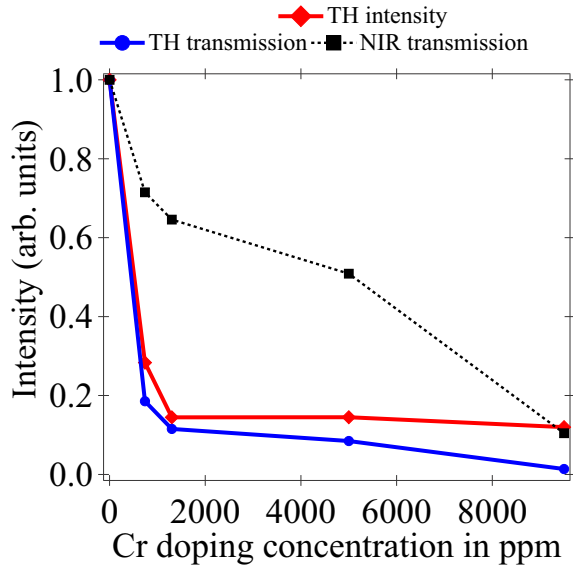
FIG. 3. The impact of doping concentration on the NIR transmission (black squares), THG intensity (red diamonds), and linear transmission of TH (blue circles) wavelength through MgO and Cr:MgO crystals. The THG intensity and transmission of NIR in crystals are measured at an estimated peak intensity of $\approx 1.0 \times 10^{13}$ W cm^{-2}. The vertical axis is normalized to unity with arbitrary units.

(VDB) and vacancies emerge in the MgO electronic band structure as a result of the Cr dopants [15–17], which can give rise to optical transitions.

The high-intensity pump laser increases the free-electron population, and the higher carrier density has been shown to affect the HHG process [18–20]. Here, the relatively short driving wavelength ensures shorter electron trajectories and a lower probability of electron-electron scattering.

B. Polarization response of THG in MgO and Cr:MgO

The driving-field polarization orientation has also been shown to reveal key signatures of the generation mechanism [6]. We have studied the linear and elliptical polarization dependences of the THG yield in the high-field regime and compared the results to perturbative and nonperturbative theories. For the details of perturbation and nonperturbation, see Appendixes A and B. To measure the linear polarization response, we keep the crystals at a fixed orientation and vary the linear polarization of the driving field using a half-wave plate (HWP). We have observed a clear anisotropic fourfold polarization response of THG in MgO and low-doped Cr:MgO (1300 ppm), whereas a more isotropic response is observed for higher-doped crystals [Cr:MgO (9500 ppm); shown in Fig. 4]. In pure MgO, You *et al.* [6] measured a more isotropic response and fourfold symmetry for THG at a field strength of 0.25 V Å^{-1} and an additional fourfold symmetry along the cubic bonding direction (Mg-O) at higher field strength (1 V Å^{-1}), leading to eightfold symmetry in total. We have observed only fourfold symmetry of THG along the O-O bonding direction at a driving wavelength of 0.8 μm of field strength (≈ 1 V Å^{-1}). Other studies have observed fourfold
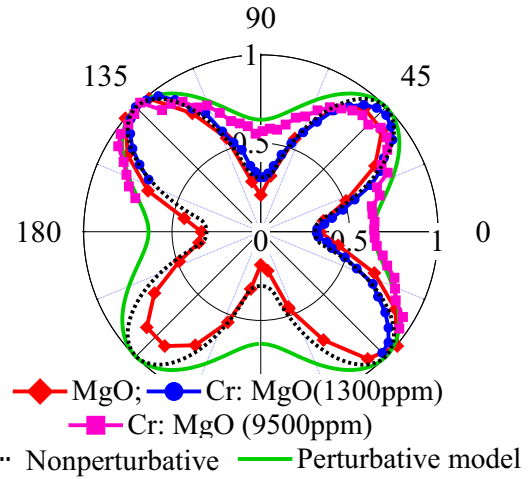

FIG. 4. Polarization response of THG in MgO (red diamonds), analytical perturbative (green line) and nonperturbative (black dotted line) models, and Cr:MgO for 1300 ppm (blue circles) and 9500 ppm (pink squares). Lines connecting the markers are used to guide the eye.

symmetry along the Mg-O direction at a driving wavelength of 1.55 μm for higher-order harmonics [13]. Comparing these studies, a complex interplay between the driving field, harmonic order, and polarization orientation is evident.

We have compared the measured polarization response of THG with the perturbative [21,22] and nonperturbative [6,10] models, as shown in Fig. 4. Perturbation theory predicts smooth TH peaks along the O-O bonding direction in MgO, coupled with isotropic emission. This theory matches well our observed polarization dependence of Cr:MgO (9500 ppm). For lower-doped and pure MgO, sharper, more defined peaks along the O-O direction emerge. This shows our data diverge from perturbative theory, and we must look to nonperturbative approaches for further insight. NP-HHG begins with the promotion of an electron from the valence band (VB) to the CB [Fig. 1(b)]. The electron then undergoes intraband oscillations or interband transitions due to the driving field, and these transitions can support the emission of higher photon energies. The crystal band structure dictates both intraband electron motion and interband transitions, making the NP-HHG sensitive to the orientation of the crystal and the polarization direction. We follow a semiclassical approach used elsewhere [6] that models single-electron motion within the conduction band of the crystal. We have followed closely the model reported in [6], i.e., that the yield of THG is dependent on the distance of the closest approach to the neighboring ionic cores in the crystal.

Other studies have shown electron-electron scattering effects can alter the HHG spectrum and should be included to interpret the spectrum [23]. Here, the short wavelength causes relatively short electron trajectories, which limits scattering effects. Electron promotion to the conduction band can, however, lead to local changes in the refractive index of the material and affect beam propagation and local intensities [24,25]. These effects are expected to have a negligible impact on the conclusions of this work.
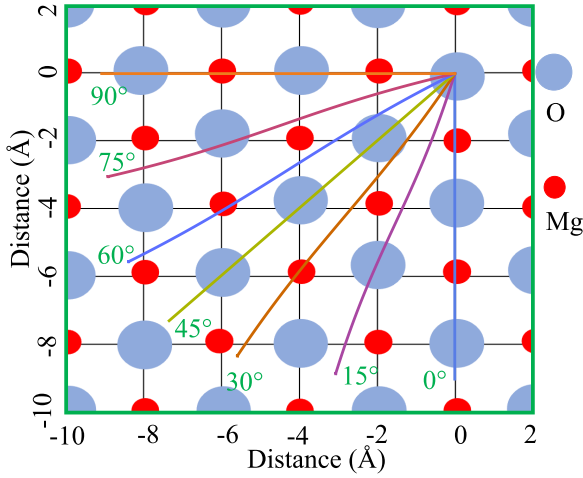
FIG. 5. The semiclassical electron trajectories for linearly polarized laser pulses for different polarization angles relative to crystal axis of MgO.

FIG. 6. Ellipticity dependence of THG in MgO and Cr:MgO. Linear polarization (vertical black dash-dotted line, $\varepsilon = 0$), elliptical polarization (vertical gray dotted line, $\varepsilon = \pm 0.5$), and circular polarization ($\varepsilon = \pm 1$). Measured response of THG in MgO (red diamonds), Cr:MgO 1300 ppm (blue circles), Cr:MgO 9500 ppm (pink squares), the perturbative model (green solid curve), and the nonperturbative model (black dotted curve). Lines connecting the markers are used to guide the eye. Linear polarization of driving field aligned (a) to the O-O bonding direction, (b) 15° away from the O-O bonding direction, (c) 30° away from the O-O bonding direction, and (d) to the Mg-O bonding direction.

The electron trajectories are calculated for a range of linear polarizations of the driving field, as shown in Fig. 5. We have considered that the electron originates from the O atoms, and the nearest neighbors to these atoms are considered for collisions. Along the cubic bonding direction (0° and 90°), the electron crosses several distinct atomic sites (Fig. 5), leading to the emission of the THG signal. As we rotate the linear polarization away from the cubic bonding direction, the intensity of the TH increases and reaches a maximum when the linear polarization is aligned in the O-O direction. As the polarization of the driving field begins to align towards the Mg-O direction, the intensity of THG decreases and returns to its minimal value. Both the numerical perturbative and non-perturbative approaches show qualitatively similar patterns. However, the measured angular polarization distribution of THG in low-doped MgO (1300 ppm) agrees with the non-perturbative model (sharper, more defined peaks), while at the highest dopant concentration (9500 ppm), the polarization response reverts to a shape better fit by the perturbative model (broader and less defined peaks). We attribute this behavior of THG to the VS to the VDB or VB transitions, as shown in Fig. 1(c). There is a possibility that THG can be observed from the CB to the VS or IDB, but it is unlikely to happen looking at the experimental data. Although the observed experimental differences in the polarization response point towards different THG mechanisms, a more robust test is required to differentiate the regimes.

C. Ellipticity dependence of THG in MgO and Cr:MgO

It has been shown elsewhere that the intensity of HHG driven by elliptically polarized driving fields is a key signature of a nonperturbative mechanism [6,8]. In the semiclassical one-electron picture, elliptical driving fields result in more curved electron trajectories in the crystal compared to linear polarization. These curved trajectories make the harmonic emission dependent on the crystal orientation and the driving-field ellipticity, causing the HHG response to differ greatly from the perturbative behavior [6,8]. We have measured the
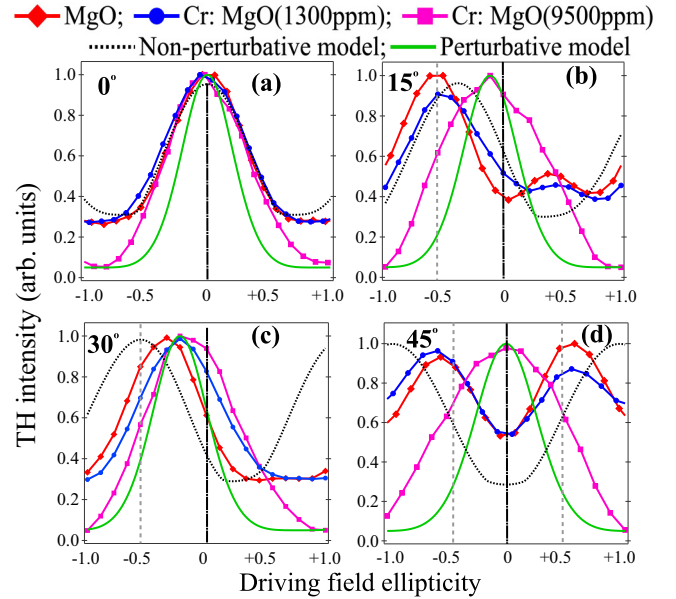
ellipticity response of THG in pure and doped MgO at four angles (0°, 15°, 30°, and 45°) between the linear polarization position of the driving field and the O-O axis of the crystals. The linear polarization of the driving field is aligned along the O-O direction with a HWP to generate the maximum THG signal. A quarter-wave plate is placed behind the HWP [as shown in Fig. 1(a)] and rotated to measure the THG intensity in a range of ellipticities. The yield of THG in pure MgO is maximum (red diamonds) for linear polarization ($\varepsilon = 0$, along the O-O axis) and minimum for circular polarization [$\varepsilon = \pm 1$; Fig. 6(a)]. It is expected that the HHG signal decreases with increasing ellipticity [8,26], as we observe with all crystals [Fig. 6(a)]; the peak-to-valley ratio is, however, much lower for the pure and low-doped crystals.

The same measurement is repeated with linear polarization of the driving field shifted by 15°, 30°, and 45° from the O-O bonding direction. At 15°, the THG peak in MgO (red diamonds) shifts from $\varepsilon = 0$ to $\varepsilon = -0.5$ in Fig. 6(b), and at 30° the peak THG signal shifts to $\varepsilon = -0.3$ [Fig. 6(c)]. At 45°, the emission peak of THG shifts from linear to elliptical ($\varepsilon = \pm 0.65$), showing a striking two-peak structure, as shown in Fig. 6(d). The shape of the Cr:MgO (9500 ppm) ellipticity dependence remains approximately centered at linear polarization for all orientations. The ellipticity dependence of THG in MgO has been compared to a perturbative model [27] and a nonperturbative model [6]. We have used Eq. (A3) to calculate the perturbative response of the ellipticity
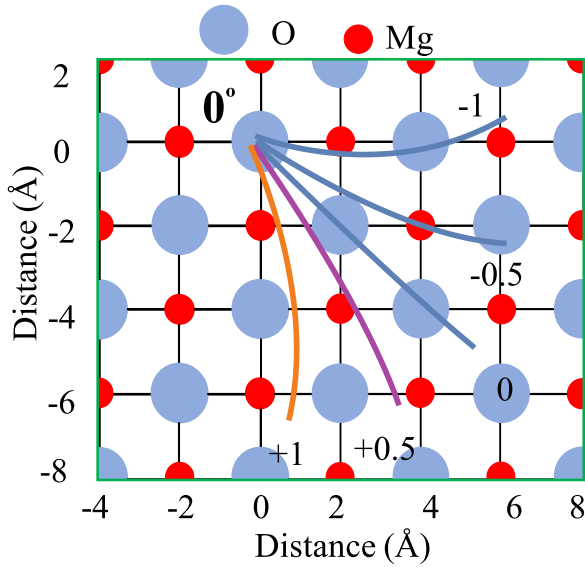
FIG. 7. The nonperturbative electron trajectories in MgO under linear (0), elliptical (±0.5), and circular (±1) polarization when the linear polarization of the driving field is considered along the O-O bonding direction.
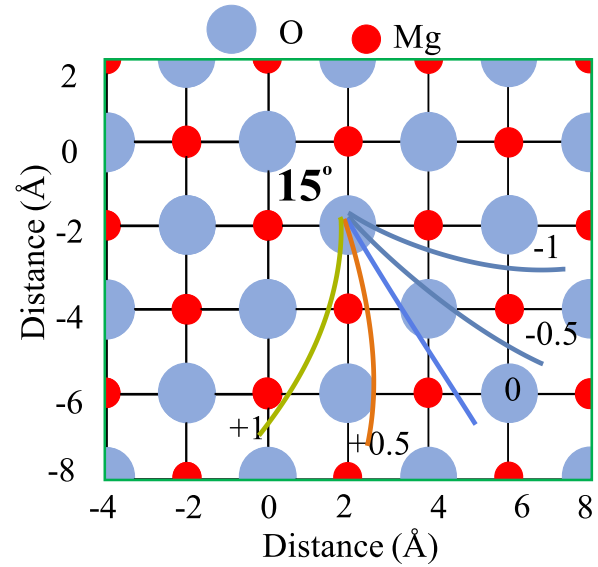

FIG. 8. The semiclassical electron trajectories in MgO under linear (0), elliptical (±0.5), and circular (±1) polarization. The linear polarization of the driving field is aligned 15° away from the O-O bonding direction.

dependence of THG. The ellipticity dependence of THG from Cr:MgO (9500 ppm) closely follows the perturbative model that predicts diminishing intensity as ellipticity increases to circular for all orientations (as shown in Fig. 6). However, the polarization responses of THG in MgO and in doped Cr:MgO (1300 ppm) closely follow the nonperturbative response.

To explain the observed nonperturbative patterns, we plot the electron trajectories in the pure MgO crystal for the 0°, 15°, 30°, and 45° orientations at a field strength of ≈1 V Å^{-1} (Figs. 7–10, respectively). In Fig. 7, the electron hits the O atomic site and results in the maximum emission of THG for $\varepsilon = 0$ [Fig. 6(a)]. Similarly, for elliptical polarization ($\varepsilon = \pm 0.5$) of the driving fields, the electron trajectory is as close to the first-neighbor Mg atom as to the second-nearest atomic site, leading to a lower TH signal. Finally, for circular polarization ($\varepsilon = \pm 1$), the electron trajectory connects only to Mg atom sites and misses the closest O atomic sites. Therefore, the contribution to the emission of TH is maximum for linear polarization and minimum for circular polarization [Fig. 6(a)]. The semiclassical electron trajectories in MgO under linear (0), elliptical (±0.5), and circular (±1) polarizations for 15° and 30° away from the O-O bonding direction are shown in Figs. 8 and 9, respectively. The ellipticity responses of THG in the high-symmetry directions (Mg-O or O-O) are symmetric around the ellipticity ($\varepsilon = 0$), while when the polarization main axis is rotated by 15° or 30° away from the O-O bond axis, the ellipticity response is anisotropic and the peak in TH yield is shifted to elliptical polarization.

Along the Mg-O bonding direction (45°), the electron trajectory first crosses a Mg atomic site for linear polarization ($\varepsilon = 0$), while for elliptical polarization ($\varepsilon = \pm 0.5$) electron trajectories miss Mg atomic sites, and for circular polarization ($\varepsilon = \pm 1$) electron trajectories are connected to the O atomic sites (see Fig. 10). Therefore, the emission of purely nonperturbative TH is minimum for linear polarization and

maximum for circular polarization [Fig. 6(d)]. The peaks for circular polarization predicted by the nonperturbative model are not observed in the experimental data for the 45° angle in Fig. 6(d). However, the deviation of peak emission to elliptical polarization depending on the angle is observed in our measurements. The nonperturbative model considers the trajectory of a single electron and does not include macroscopic aspects, such as phase matching, that will be minimized for circular polarization in all cases. The ellipticity response of the Cr:MgO (9500 ppm) crystal is congruent with
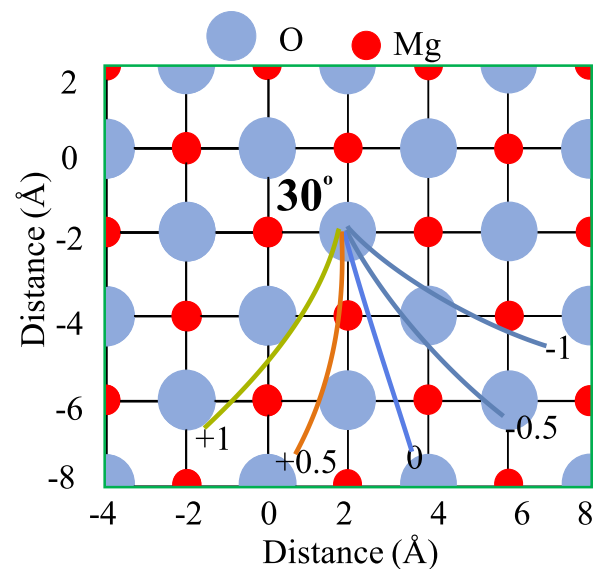

FIG. 9. The semiclassical electron trajectories in MgO under linear (0), elliptical (± 0.5), and circular (±1) polarization. The linear polarization of the driving field aligned 30° away from the O-O bonding direction.
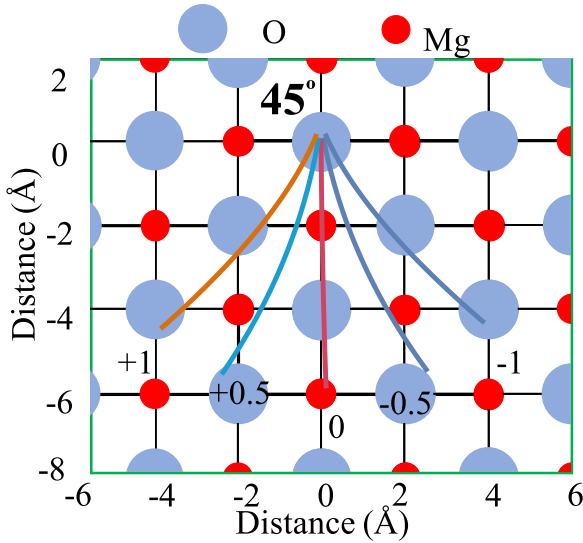
FIG. 10. The nonperturbative electron trajectories in MgO under linear (0), elliptical (±0.5), and circular (±1) polarization when the linear polarization of the driving field is kept along the Mg-O bonding direction.

the expected perturbative response. The marked deviation of the driving-field ellipticity response in pure and low-doped MgO, however, cannot be explained by perturbative theory, whereas a satisfactory match with the NP-HHG model is found.

This behavior can be explained in terms of the electron structure of pure and doped MgO. The Cr dopants change the electronic structure of pure MgO and change the possible direct electron transitions (interband) and electron trajectories (intraband). In pure MgO, an electron is the first field ionized from the VB to CB, where the electron is driven by the field and its oscillations cause NP-THG [Fig. 1(b)]. In Cr:MgO, however, new energy levels appear between the VB and CB and within the CB itself [13,14]. Although we have approximated the Cr:MgO band structure here, it is in broad agreement with other works [13,14]. Moreover, the observed increased absorption of the NIR and TH frequencies in Fig. 3 are consistent with the approximation. The new levels allow single-photon transitions from the VS to CB and split the CB by Cr levels (Fig. 1(c), effectively blocking long-range intraband oscillations in lieu of single-photon intraband transitions. Therefore, at high Cr doping concentrations, the NP-THG mechanisms are greatly limited by the introduction of new energy levels causing linear absorption of the driving photons and blocking long-range pathways of the free electrons. The remaining available THG mechanism in these crystals is perturbative and occurs either between the VS and CB or VDB or between the CB and VS or IDB. The most probable transition would be between the VS and VDB or VB as the THG from this transition agreed well with our experimental data. In the Cr:MgO (9500 ppm) crystal, the ellipticity dependence follows the purely perturbative predictions, whereas in pure and low-doped MgO, the electron motion within the conduction band causes NP-THG, which can be explained in terms of intraband electron motion.

IV. CONCLUSIONS

Although THG is generally assumed to be perturbative, we have shown that in the right conditions, NP-THG can be generated in wide-band-gap insulators such as MgO using 800-nm light. The intensity scaling measurements validate the nonperturbative response of THG in pristine and low-doped MgO, whereas higher-doped MgO exhibits a perturbative response of THG in the high-field regime. We have confirmed this behavior by comparing the pure MgO results to crystals with increasing levels of dopants that alter the electronic structure. As dopant concentration is increased, the pathways for NP-THG to occur decrease, and the pathways for linear absorption of the driving field increase, which ultimately results in a largely perturbative response.

This study shows that even the lowest odd-harmonic order can originate from a nonperturbative process and that the emission intensity is sensitive to the electronic and crystal structure. Moreover, the nonperturbative process allows for significantly more emission of circularly polarized light than a traditional perturbative THG, which could be an attractive probe to study chiral materials, molecules, and magnetic materials.

APPENDIX A: PERTURBATIVE MODEL

The anisotropic THG linear polarization response is compared with the perturbative model [21,22]. The third-order polarization for a cubic crystal with $m3m$ symmetry is given as [28]

$$P_i(3\omega) = 3\chi_{xxyy}E_i(EE) + (\chi_{xxxx} - 3\chi_{xxyy})E_iE_iE_i, \quad (A1)$$

where i refers to the three cubic axes. The intensity of THG for the s-polarized driving field is given as

$$I_{ss}(3\omega)\alpha[(\chi_{xxxx} - 3\chi_{xxyy})\cos(4\phi)$$
$$+ 3(\chi_{xxxx} + \chi_{xxyy})]^2|E_s(\omega)|^6. \quad (A2)$$

In Eq. (A2), $E_s(\omega)$ and $I_{ss}(3\omega)$ are the s-polarized driving electric field and intensity of THG, ϕ is the angle between the crystal axis and the s-polarized electric field $E_s(\omega)$, and $|3(\chi_{xxxx} + \chi_{xxyy})|^2$ and $|(\chi_{xxxx} - 3\chi_{xxyy})|^2$ are the isotropic and anisotropic contributions to the nonlinear response, respectively. For the best fit of this perturbative response to our experimental THG polarization response, the isotropic and

anisotropic terms are chosen to be 0.006 and $2.76 \times e^{-6}$ [29], respectively.

The ellipticity dependence of THG in MgO has been compared to the perturbative model [27]. According to the perturbative model, the intensity of harmonic q is given as

$$I_q = I_{q0} + \gamma \left(\frac{1 - \epsilon^2}{1 + \epsilon^2} \right)^{q-1}, \tag{A3}$$

where I_{q0} corresponds to baseline harmonic intensity and γ, q, and ϵ are the proportional factor, harmonic order, and laser field ellipticity, respectively.

APPENDIX B: NONPERTURBATIVE MODEL

The nonperturbative model is based on the semiclassical analysis of electron trajectories in the conduction bands of the crystal as described previously [6]. A semiclassical analysis of electron trajectories inside a crystal of MgO for linear and elliptical polarizations has been reported [6]. According to the semiclassical model, the motion of an electron in the energy band under the influence of the driving laser field $E(t) = E_0 \cos(\omega t)$ is given as

$$\frac{d\overrightarrow{k}}{dt} = -\overrightarrow{E}(t), \tag{B1}$$

where k is the crystal momentum. The evolution of the position of an electron wave packet in the conduction band can be given as

$$\frac{d\overrightarrow{r}}{dt} = \frac{\partial \varepsilon(\overrightarrow{k})}{\partial(\overrightarrow{k})}, \tag{B2}$$

where $\varepsilon(\overrightarrow{k})$ is the conduction-band energy dispersion. For the face-centered crystal, the energy dispersion of the crystal in the (001) plane is approximated by the tight-binding model

and is expressed as

$$\varepsilon(k_x, k_y; k_z = 0) = 3(A + B) - A\left[\cos\frac{k_x a}{2} + \cos\frac{k_y a}{2} \right.$$
$$\left. + \cos\frac{k_x a}{2}\cos\frac{k_y a}{2} \right] - B[1 + \cos(k_x a) + \cos(k_y a)].$$

Here, A and B are constants which are chosen to fit the structure of the crystals. We used $A = 1.25$ and $B = 0.6$, as given by Tan *et al.* [30], to match the structures of MgO.

The quantitative harmonic yield cannot be predicted by these semiclassical electron trajectories, but this analytical analysis is quite useful to predict the angular distribution of the harmonics. We follow the same assumptions for our calculation in pure MgO as reported in [6], i.e., that the yield of THG is essentially dependent on the closeness of the trajectories of the electron regarding ionic cores in the crystal. To that end, we considered Gaussian symmetrical charge distributions around the ionic cores. The yield of high harmonics is calculated as

$$I_{\mathrm{HHG}} \propto C_{mg}e^{-\frac{(r - r_{mg})^2}{a_{mg}^2}} + C_o e^{-\frac{(r - r_o)^2}{a_o^2}}, \tag{B3}$$

where C_o and C_{mg} are the strengths of the harmonic emission corresponding to the collisions with the magnesium and oxygen atom, a_o and a_{mg} are the size of the ionic cores, and r_o and r_{mg} are the location of the ionic cores of oxygen and magnesium, respectively. r is the closest distance of the electron from the center of the ionic core. By using this semiclassical model, You *et al.* [6] chose $C_0 = 0.15$ and $C_{mg} = 1$ to match the relative maxima along the O-O and Mg-O directions for the 21st harmonics, while $a_o = 0.35a$ and $a_{mg} = 0.1a$ were taken from Ref. [31], where $a = 4.2$ Å is the lattice constant of MgO. We have chosen $C_0 = 1$ and $C_{mg} = 0.05$ and $a_o = 0.35a$ and $a_{mg} = 0.1a$ to match the relative maxima along O-O and minima along the Mg-O directions for the third harmonics in MgO under an electric field strength of ≈ 1.0 V/Å.

[1] M. C. Kohler, T. Pfeifer, K. Z. Hatsagortsyan, and C. H. Keitel, Frontiers of atomic high-harmonic generation, Adv. At., Mol., Opt. Phys. **61**, 159 (2012).

[2] S. Ghimire, A. D. DiChiara, E. Sistrunk, P. Agostini, L. F. DiMauro, and D. A. Reis, Observation of high-order harmonic generation in a bulk crystal, Nat. Phys. **7**, 138 (2011).

[3] P. A. Franken, A. E. Hill, C. W. Peters, and G. Weinreich, Generation of Optical Harmonics, Phys. Rev. Lett. **7**, 118 (1961).

[4] J. Wildenauer, Generation of the ninth, eleventh, and fifteenth harmonics of iodine laser radiation, J. Appl. Phys. **62**, 41 (1987).

[5] T. T. Luu, M. Garg, S. Y. Kruchinin, A. Moulet, M. T. Hassan, and E. Goulielmakis, Extreme ultraviolet high-harmonic spectroscopy of solids, Nature (London) **521**, 498 (2015).

[6] Y. S. You, D. A. Reis, and S. Ghimire, Anisotropic high-harmonic generation in bulk crystals, Nat. Phys. **13**, 345 (2017).

[7] N. Tancogne-Dejean, O. D. Mücke, F. X. Kärtner, and A. Rubio, Impact of the Electronic Band Structure in High-Harmonic Generation Spectra of Solids, Phys. Rev. Lett. **118**, 087403 (2017).

[8] N. Tancogne-Dejean, O. D. Mücke, F. X. Kärtner, and A. Rubio, Ellipticity dependence of high-harmonic generation in solids originating from coupled intraband and interband dynamics, Nat. Commun. **8**, 745 (2017).

[9] M. Wu, Y. You, S. Ghimire, D. A. Reis, D. A. Browne, K. J. Schafer, and M. B. Gaarde, Orientation dependence of temporal and spectral properties of high-order harmonics in solids, Phys. Rev. A **96**, 063412 (2017).

[10] Y. S. You, J. Lu, E. F. Cunningham, C. Roedel, and S. Ghimire, Crystal orientation-dependent polarization state of high-order harmonics, Opt. Lett. **44**, 530 (2019).

[11] G. Vampa, C. R. McDonald, G. Orlando, D. D. Klug, P. B. Corkum, and T. Brabec, Theoretical Analysis of High-Harmonic Generation in Solids, Phys. Rev. Lett. **113**, 073901 (2014).

[12] J. Seres, E. Seres, C. Serrat, and T. Schumm, Non-perturbative generation of DUV/VUV harmonics from crystal surfaces at 108 MHz repetition rate, Opt. Express **26**, 21900 (2018).

[13] V. E. Nefedova, S. Fröhlich, F. Navarrete, N. Tancogne-Dejean, D. Franz, A. Hamdou, S. Kaassamani, D. Gauthier, R. Nicolas,

G. Jargot, M. Hanna, P. Georges , M. F. Ciappina, U. Thumm, W. Boutu, and H. Merdji, Enhanced extreme ultraviolet high-harmonic generation from chromium-doped magnesium oxide, Appl. Phys. Lett. **118**, 201103 (2021).

[14] M. Hussain, H. Pires, W. Boutu, D. Franz, R. Nicolas, T. Imran, H. Merdji, M. Fajardo, and G. O. Williams, Controlling the non-linear optical properties of MgO by tailoring the electronic structure, Appl. Phys. B **126**, 46 (2020).

[15] M. Henry, J. Larkin, and G. Imbusch, Nature of the broad-band luminescence center in MgO:Cr^{3+}, Phys. Rev. B **13**, 1893 (1976).

[16] L. N. Kantorovich, A. L. Shluger, and A. M. Stoneham, Recognition of surface species in atomic force microscopy: Optical properties of a Cr^{3+} defect at the MgO (001) surface, Phys. Rev. B **63**, 184111 (2001).

[17] F. Stavale, N. Nilius, and H.-J. Freund, Cathodoluminescence of near-surface centres in cr-doped MgO (001) thin films probed by scanning tunnelling microscopy, New J. Phys. **14**, 033006 (2012).

[18] Z. Wang, H. Park, Y. H. Lai, J. Xu, C. I. Blaga, F. Yang, P. Agostini, and L. F. DiMauro, The roles of photo-carrier doping and driving wavelength in high harmonic generation from a semiconductor, Nat. Commun. **8**, 1686 (2017).

[19] C. Heide, Y. Kobayashi, A. Johnson, F. Liu, T. F. Heinz, D. A. Reis, and S. Ghimire, Probing electron-hole coherence in strongly-driven solids, arXiv:2109.04508.

[20] K. Nagai, K. Uchida, S. Kusaba, T. Endo, Y. Miyata, and K. Tanaka, Effect of incoherent electron-hole pairs on high harmonic generation in atomically thin semiconductors, arXiv:2112.12951.

[21] J. E. Sipe, D. J. Moss, and H. M. van Driel, Phenomenological theory of optical second-and third-harmonic generation from cubic centrosymmetric crystals, Phys. Rev. B **35**, 1129 (1987).

[22] G. Petrocelli, E. Pichini, F. Scudieri, and S. Martellucci, Anisotropic effects in the third-harmonic-generation process in cubic crystals, J. Opt. Soc. Am. B **10**, 918 (1993).

[23] C.-M. Wang, N. Tancogne-Dejean, M. Altarelli, A. Rubio, and S. A. Sato, Role of electron scattering on the high-order harmonic generation from solids, Phys. Rev. Research **2**, 033333 (2020).

[24] M. Hussain, S. Kaassamani, T. Auguste, W. Boutu, D. Gauthier, M. Kholodtsova, J.-T. Gomes, L. Lavoute, D. Gaponov, N. Ducros, S. Fevrier, R. Nicolas, T. Imran, P. Zeitoun, G. O. Williams, M. Fajardo, and H. Merdji, Spectral control of high order harmonics through non-linear propagation effects, Appl. Phys. Lett. **119**, 071101 (2021).

[25] M. Hussain, G. O. Williams, T. Imran, and M. Fajardo, Non-linear propagation effects of intense femtosecond pulses on low order harmonics in solids, arXiv:2104.10629.

[26] N. Klemke, N. Tancogne-Dejean, G. M. Rossi, Y. Yang, F. Scheiba, R. Mainz, G. Di Sciacca, A. Rubio, F. X. Kärtner, and O. D. Mücke, Polarization-state-resolved high-harmonic spectroscopy of solids, Nat. Commun. **10**, 1319 (2019).

[27] G. P. Zhang and T. F. George, Ellipticity dependence of optical harmonic generation in C_{60}, Phys. Rev. A **74**, 023811 (2006).

[28] W. Burns and N. Bloembergen, Third-harmonic generation in absorbing media of cubic or isotropic symmetry, Phys. Rev. B **4**, 3437 (1971).

[29] F. Abrinaei, Nonlinear optical response of Mg/MgO structures prepared by laser ablation method, J. Eur. Opt. Soc. Rapid Publ. **13**, 15 (2017).

[30] Y. Tan, M. Povolotskyi, T. Kubis, Y. He, Z. Jiang, G. Klimeck, and T. B. Boykin, Empirical tight binding parameters for GaAs and MgO with explicit basis through DFT mapping, J. Comput. Electron. **12**, 56 (2013).

[31] Y.-N. Xu and W. Y. Ching, Self-consistent band structures, charge distributions, and optical-absorption spectra in MgO, α-Al_2O_3, and $MgAl_2O_4$, Phys. Rev. B **43**, 4461 (1991).